PERGAMON

Planetary and Space Science 49 (2001) 645–656

Planetary and Space Science

www.elsevier.nl/locate/planspasci

Sputtering of the Martian atmosphere by solar wind pick-up ions

F. Leblanc *, R.E. Johnson

Engineering Physics and Department of Astronomy, University of Virginia, 102, Charlottesville, VA 22903, USA

Received 18 May 2000; received in revised form 27 November 2000; accepted 1 December 2000

Abstract

Monte Carlo models are used to describe the interaction between the incident pick-up ions and the Mars neutral atmosphere. The sputtered population inside the corona and escaping particles are described using a modified 3D test particle model, whereas, the heating effect due to the incident flux is described using a 2D Direct Simulation Monte Carlo. These results show that the standard 1D models overestimate the sputtering yield (by 15–25%), when corrected for coronal ejection. It is also shown that the exobase altitude can depend on sputtering. Two epochs of Mars history are simulated. For an epoch suggested to be about 2.5 Gyr ago, sputtering is at least as important as dissociative-recombination for populating the corona and the heating due to the pick-up ion flux is of the same order as the EUV and UV heating of the thermosphere. For this epoch and present solar minimum conditions we present the distribution in the density and the energy of the sputtered particles in Mars corona. In particular we show that the polar and dusk regions are the most dense regions and the shadow of the dawn and polar regions the most energetic regions.

1. Introduction

Most scenarios for the evolution of Mars (Pepin, 1994; Carr, 1999) assume that water was a stable element on the surface in an earlier era (Zuber et al., 2000). This implies that Mars was wetter, warmer and had a thicker atmosphere than today. It is not yet understood when or how the water disappeared. The various scenarios for the loss of water agree on the following main phases of the atmospheric evolution. Before 4.4 Gyr from present, strong hydrodynamic escape, heavy bombardment of meteorites and outgassing have been used to describe Mars atmospheric evolution (Brain and Jakosky, 1994). The heavy bombardment may have lasted until 3.7 Gyr ago ending about the same time that the magnetic field of Mars turned off (Acuña et al., 1999, 1998; Carr, 1999). Impact bombardment and early hydrodynamic escape is estimated to have caused a loss of roughly 90% of the primitive Martian volatiles. However, impact surface features show a strong degradation due to erosional processes (Jakosky and Jones, 1997) suggesting that water was still present at the end or after the heavy bombardment period.

Carr (1999) has suggested that a 1–0.5 bar thick atmosphere should have been present after the heavy bombardment period. He also emphasized that one of the main factors which could explain the present much thinner 5 mb atmosphere is the sputtering of the atmosphere by pick-up ions, first described by Luhmann and Kozyra (1991). Photochemical escape (McElroy, 1972; Zhang et al., 1993a) and carbonate recycling (CO_2 deposited in a near surface reservoir) could also contribute. Jakosky and Jones (1997) concluded from the analysis of the present isotope ratios that 85–90% of Ar, C, H and N may have been lost by sputtering. The purpose of this work is to describe the 3D nature of the sputtering process in two epochs: the present solar minimum and an epoch suggested to be 2.5 Gyr ago to the present. The ultimate goal is to calculate whether or not sputtering determined the CO_2 and oxygen composition of the atmosphere and contributed to the inferred loss of 0.95–0.45 bar of atmosphere (Carr, 1999).

Whereas, the sputtering of Io's atmosphere was a well studied process (e.g., see Johnson, 1994; Smyth and Combi, 1988), the sputtering of the Martian atmosphere by *pick-up ions* was first described by Luhmann and Kozyra (1991). On the dayside, solar EUV and photo-electrons ionize a fraction of the neutral atmosphere. Because of the absence of a large permanent magnetic field, these newly ionized particles are picked-up by the partially deflected field frozen in the solar wind. They are accelerated along gyroradial trajectories in the Martian tail direction and some of them reimpact the

* Correspondence address: Service d'Aeronomie du CNRS, 91371 Verrieres le Buisson Cedex BP 3, France. Tel.: +33-1-64474303; fax: +33-1-69202999.

E-mail address: francois.leblanc@aerov.jussieu.fr (F. Leblanc).

0032-0633/01/$ - see front matter
PII: S0032-0633(01)00003-4

neutral atmosphere and collide with neutral particles with sufficient energy to generate new ejecta and ballistic particles. The net loss of atmosphere due to this mechanism has been estimated in several papers (Jakosky et al., 1994; Kass and Yung, 1995, 1996; Johnson and Liu, 1996; Johnson et al., 2000). But these have all been 1D models and the potential feedback processes been treated approximately (Johnson and Luhmann, 1998). That is, the sputtered neutral particles increase the corona density where they can be ionized and can form additional pick-up ions liable to reimpact the neutral atmosphere. Johnson and Luhmann (1998) estimated the density of sputtered particles in the corona and concluded the feedback process could significantly increase the loss of atmosphere due to the sputtering during the period from the time the Martian magnetic field decayed to the present. The principal purpose of this work is to use a 3D Monte Carlo simulation to test the validity of the 1D models of atmospheric sputtering. Therefore, we provide a new estimate of the average number of ejected neutrals generated by an incident particle. A second purpose is to re-calculate the importance of the coronal density enhancement produced by sputtering. The 3D approach allows us to treat all incident angles for the pick-up ions and to determine the horizontal structure of the sputter-produced corona.

In Section 2 we describe the Monte Carlo models and in Section 3 we quantify the effect of sputtering in two epochs. These results depend critically on the pick-up ion fluxes initially estimated by Zhang et al. (1993a) but the calculated yields can be applied when more accurate pick-up ion fluxes are available. In the last section, we present our conclusions.

2. Monte Carlo simulations

In order to model the interaction of the incident pick-up ions with the Martian neutral particles we developed a 3D Monte Carlo (MC) simulation which follows the incident particles when they penetrate the neutral atmosphere and describes the cascade of collisions and recoil particles that are generated. We also use a 2D Direct Simulation Monte Carlo (DSMC, see Bird, 1994) to describe more accurately the effect of this interaction on the atmosphere below the exobase. Both approaches are based on the same model. Since the number of real particles in the atmosphere or in the incident flux is too large, in the Monte Carlo approach one assumes that a simulated particle represents a large number of real particles. In this work, each tracked particle typically represents between 10^{25} and 10^{28} real particles. This number, called the weight of the particle, is an important parameter of the simulation since it also fixes the density of simulated recoil particles due to the flux of incident particles. These in turn determine the accuracy with which the cascade of energy due to an incident particle is described. Rather than use different weights for these particles we break the problem into two pieces because the majority of the particles are slow and it is primarily the few fast ones that populate the corona. In the 3D Monte Carlo simulation, only particles with a kinetic energy above a certain energy are followed in order to limit the computing time and low energy particles, roughly, an energy lower than 0.1 eV, are not followed in this model. The main consequence of such simplification is that the MC model does not self-consistently describe the heating of the neutral atmosphere due to the bombardment by the keV ions. In the present epoch, this assumption is justified by the fact that UV and EUV heating are more efficient. Therefore, for the present period, we use the model of atmospheres developed by Zhang et al. (1993a), Bougher and Roble (1991) and Bougher et al. (1999). However, for the period 2.5 Gyr ago, the sputter heating can have an important effect on the altitude of the exobase, mainly in the subsolar regions (e.g., Pospiezalska and Johnson, 1992, 1996; Wong and Johnson, 1995). This increase of the exobase radius implies that a larger surface area of Mars atmosphere is submitted to the flux of pick-up ions and it can change the position of the population above the ionopause. We determine the heating of the atmosphere by the energetic incident particles using a 2D-DSMC code. In this model, all the simulated particles are followed. Starting with the Zhang et al. atmosphere (1993a) for the earlier epochs, the results of this simulation define the neutral atmosphere for the 3D Monte Carlo model. The latter is then used to determine the characteristics of the sputtered population (coronal density enhancement and sputtering yield).

The incident pick-up ions, mainly O^+ and H^+ (Luhmann and Kozyra, 1991; Brecht 1997a, b), are efficiently neutralized before reaching the exobase, which is defined as the altitude above which collisions are unlikely (Luhmann and Kozyra, 1991; Johnson et al., 2000). Indeed, the collision cross section for charge exchange is typically one order larger than that for "knock-on" collisions (collision which generates significant exchange of momentum). Our Monte Carlo models then describe high-energy incident neutral particles moving only under the effect of the Mars gravity field and interacting with low-energy neutrals in the Martian atmosphere. We follow these particles above an altitude from the Mars surface such that any incident particle reaching this altitude has only a small effect. Such particles generate only recoil particles which will be thermalized quickly and do not contribute to the heating near the exobase, to the corona or to the total escape (Johnson et al., 2000).

In both MC and DSMC approaches, the collisions are binary. Such collisions can happen between two fast particles (recoil or incident particles) or between a fast particle and a background atmospheric particle. The number of collisions is determined by our choice of maximum impact parameter, 2.5 Å . This impact parameter was chosen to optimize the sputtering calculation as discussed in Johnson et al. (2000). It corresponds to an energy transfer greater than 50% of the energy of the incident particle in the case of a 0.07 eV particle, greater than 5% in the case of a particle of 2 eV and greater than 0.5% for a 20 eV particle. We then neglect the collisions which are associated with small energy transfer.

The particle tracking is described following the algorithm of Bird (1994). The domain where we follow the particles is divided into cells and the motion of the particles is described as follows:

- At a time t of the simulation, we calculate the displacement of the fast particles for a chosen time step $\mathrm{d}t$. $\mathrm{d}t$ is chosen in order that the fastest particle moves less than the smallest distance between two boundaries of the smallest cell.
- At $t + \mathrm{d}t$, in each cell, the probability that a collision occurs between fast/fast or fast/background atmospheric particles is determined from the volume of the cell, the effective collision cross section for fast/fast and fast/background particles, respectively, the densities in the cell of both types of particles, the average relative speed between the particles and the time step $\mathrm{d}t$. The average relative speed between particles is sampled during the simulation. From the computed probability, the average number of pairs which collide is determined. Pairs of colliding particles are selected randomly and a test on their relative speed is made to reproduce the average number of collisions which should statistically happen between the time t and $t + \mathrm{d}t$ in each cell (Bird, 1994). If a collision is selected, the velocities of the two particles after a collision is calculated using a universal potential of interaction (Johnson et al., 2000; Ziegler et al., 1985). An electronic energy loss (Johnson et al., 2000; Firsov, 1959) is also included which takes into account the energy lost by the colliding particles due to interaction with the electrons of each impactors. When all the collision calculations which should occur have been performed, all the particles are moved ballistically for a new period $\mathrm{d}t$ without encountering further collisions.

The particles are followed and the collisions are described as long as these particles remain between the lower boundary (140 km for present time and 150 km for earlier epoch) and an arbitrary altitude (400 km for present time and 600 km for earlier epochs) chosen higher than the exobase altitude. When they cross the lower boundary, they are suppressed, since we consider that at such an altitude these particles are quickly thermalized. When they cross the upper boundary, they become ballistic particles which are subject only to the Martian gravity field. These coronal particles are followed until they either again cross the upper boundary of the domain that we consider as collisional where they are reintegrated inside the population of colliding fast particles, or until they reach a distance of $2R_{\mathrm{m}}$ from the Mars surface above which we suppress them. Indeed, these particles represent only a small part of the coronal particles and have a non-negligible probability for ionization or drag by the solar wind before returning to $2R_{\mathrm{m}}$. Actually, around $1/3$ of them are ionized by photo-ionization, charge exchange or electron impact before coming back below $2R_{\mathrm{m}}$, but their contribution to the corona density when they come back in it is small and is neglected in the following results.

The main difference between the 3D-MC simulation and the 2D-DSMC simulation is that low-energy particles (typically energy below 0.1 eV) are assumed to be frozen in the former. Indeed one of the goals of this work is to determine the importance of the potential feedback process: ionization of the neutral particles sputtered into the corona. This requires a 3D approach because Mars' rotation changes significantly the corona. A full 3D-DSMC which includes the coronal particles and describes the heating of the thermosphere is computationally too expensive at present. Luhmann and Kozyra (1991) show that the newly ionized particles which can reimpact and efficiently sputter the neutral atmosphere mainly originated from altitudes much higher than the exobase in order for them to be accelerated sufficiently before colliding with atmospheric particles. Zhang et al. (1993a) in an overly simple field model assume that the ionization mainly takes place above the ionopause. These authors considered photo-ionization, charge exchange and electron impact, with the last process being the most efficient process for ionization of the O atom in the Martian corona. Therefore, we need to describe accurately the enhancement of the corona density above the ionopause. For this reason, in the 3D MC code, we only follow the particles which have enough energy to reach such an altitude. In the present epoch, the ionopause is estimated to be roughly at 300 km at the subsolar point and 700 km in the pole (Zhang et al., 1993a; Hodges, 2000). For the earlier epoch, the ionopause altitude should be similar to the present one since the atmosphere is thicker than at present (roughly one-order higher density at 300 km) but with a 1–3 times more intense solar wind (Johnson and Luhmann, 1998; Zhang et al., 1993a). The energy threshold, we used in this simulation, is defined such that a particle of lower kinetic energy than some fraction of the escaping energy is not followed. This threshold fixes the average number of recoil particles which have to be followed at each time step, which is directly linked to the computing time of the simulation. This in turn determines an altitude above which the 3D aspects of the corona are well described.

3. The 1EUV and 3EUV epochs

Zhang et al. (1993a) have defined three different periods for the solar activity history. For each period the flux of solar EUV radiation is given in terms of the present EUV flux at solar minimum (1EUV). The 6EUV period was assumed to correspond to a very early epoch of the solar system with an EUV flux 6 times greater than the present. During this period Mars may have had a field (Acuña et al., 1999) and if not feedback processes dominate the interaction between pick-up ions and Mars' atmosphere. We will then not consider this period in this present work. The 3EUV flux is assumed to correspond roughly to the period

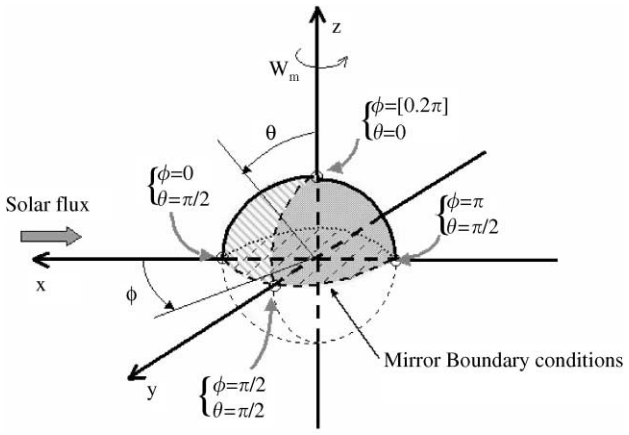

Fig. 1. Coordinate system. The half-upper part is the domain of calculation, the clear dashed part is the domain bombarded by the incident flux and the darker part the non-bombarded one.

around 2.5 Gyr ago at a time at which the magnetic field had already decayed leaving a remanent field not strong enough to protect the Mars atmosphere from the incident pick-up ions. In this paper, the effect of the pick-up ions on the atmosphere is calculated at 1EUV and 3EUV.

The real flux of pick-up ions is fully 3D according to Brecht (1997a, b). However, for comparison with earlier results, we used the over-simplified model defined by Zhang et al. (1993a) and used by Luhmann et al. (1992). This flux is assumed to be uniform across a surface perpendicular to the Mars/Sun axis. The particles are all assumed to be O^+ ions with 1 keV energy. Any contribution of H^+ is neglected because these particles have a small sputtering effect since their mass is small compared to the average mass of the atmospheric particles (Luhmann and Kozyra, 1991). However, the proton flux may add considerable heat (Kallio and Luhmann, 1997; Brecht, 1997b) and will be described in future work. The flux used in this simulation is equal to 5×10^5 ions cm^{-2} s^{-1} for the present epoch at solar minimum (1EUV) and 9×10^7 ions cm^{-2} s^{-1} for the period starting 2.5 Gyr ago (3EUV). The later is larger than present solar maximum conditions.

Since the flux of pick-up ions used in this simulation is symmetric around the Sun/Mars axis, we will simulate half the atmosphere of Mars and will introduce a mirror boundary condition to describe the whole atmosphere (Fig. 1). A 3D model is needed because calculating the coronal density due to the sputtered population implies that several Mars days have to be simulated since the coronal particles have velocity of the order of Mars' rotation. Therefore, Mars' rotation has been introduced. The coordinate system (x, y, z) is centered on Mars with x always directed towards the Sun and z with the same orientation as Mars' rotation vector. In this paper, we neglect the 25° of obliquity of the Mars rotation axis with respect to the ecliptic plane. Indeed, over one year the average angle between the rotation axis and the Solar incident flux is equal to 90°. A test including the obliquity of Mars has been performed and has provided no significant changes compared to the case without it. We also defined a spherical coordinate system (r, θ, ϕ) where r is the distance from the center of Mars, θ is the angle between the vector considered and the z axis and ϕ is the angle between the x axis and the projection of this vector on the Mars orbital plane (xy). θ varies from 0 at the pole to $\pi/2$ at the equator and ϕ varies from 0 at the subsolar point (12 a.m. Mars local time) to 2π. $\phi = \pi$ corresponds to 12 p.m. Mars local time. $\theta = \pi/2$ corresponds to the plane defining the mirror boundary condition (Fig. 1).

The space around Mars in which we follow the particles is divided into cells which are distributed exponentially in the radial (r) direction (in order that each cell contains roughly the same number of atmospheric particles) and equally distributed in the latitude (θ) and longitude (ϕ) directions, respectively, 20, 20 and 80 cells for the radial, latitudinal and longitudinal directions in the domain penetrated by the ions. Above this domain until $2R_m$ the space is covered by a grid distributed in the same way and with $50 \times 20 \times 80$ cells. The calculation of the density of fast particles and the collision rate in the 3D MC model is based on the assumption that a stationary state of the ballistic and escaping particles is reached after a few Mars rotations (typically, three rotations is enough to reach such a stationary state). The time spent and the collisions made by fast particles inside a cell are accumulated. The final density of particles and rate of collision are then calculated at the end of the simulation by dividing by the total time of the simulation and by converting the result into a real density by taking into account the volume of the cells and the weight of the simulated particles.

3.1. *1EUV*: *present solar minimum conditions*

The Martian atmosphere in the present epoch (solar minimum) has been characterized by Mars Thermospheric Global Circulation Model (MTGCM) 3D upper atmosphere–ionosphere model of Bougher et al. (1991, 1999) and by Zhang et al. (1993a). The MTGCM model includes the effect of the UV and EUV solar flux, the chemistry for CO_2, CO, N_2, O_2, Ar and O molecules and O_2^+, CO_2^+ and O^+ ions and the global dynamics between the dayside/nightside for solar maximum and minimum. Zhang et al. (1993a) use a 1D model which describes the density and temperature profiles of the atmosphere based on a 1D two stream model (Nagy and Cravens, 1988). In this paper, we use the density profiles of Zhang et al. (1993a) and the temperature profiles of Bougher et al. (1999) to define the neutral atmosphere. These profiles are in agreement with the measurements made by the Martian probes and by airglow measurements. A dayside/nightside dependence of the temperature is introduced following the work of Bougher et al. (1999). We simplify the description of the neutral atmosphere by assuming that a molecule of CO_2 is equal to three individual atoms of oxygen and then by considering

that the atmosphere consists only of O atoms. This assumption is discussed in Johnson et al. (2000) and in the corona for the 1EUV epoch O oxygen dominates CO_2 above 205 km (Zhang et al., 1993a). The corresponding density and temperature are deduced from CO_2 and O profiles. This last assumption implies that the loss estimate presented in this work is an upper bound of the real one (Johnson et al., 2000).

The 3D collisional domain described for the fast recoils is between 140 and 400 km in altitude, above which particles are in ballistic trajectories. The background Martian atmosphere consists of 5×10^{33} real particles. For this simulation, we used a weight factor equal to 2×10^{25} and followed 2898 incident particles simulating the bombardment of the atmosphere. The energy threshold used is $\sim$ 0.07 eV (or $\sim$ 700 K). For comparison, the exospheric temperature on the dayside as determined by Bougher et al. (1999) is equal to 209 K. This energy means that the corona is accurately described above 320 km since we follow all the particles which have enough energy to reach such altitude. This estimate is close to the ionopause altitude, 300 km, calculated in Zhang et al. (1993a).

Because collisions above 200 km primarily affect the lower energy recoils, the standard estimate of the exobase altitude applies, $n/(\sigma_d H) = 1$, where n is the density, σ_d is the momentum transfer cross section between the fast and the atmospheric particles and H is the scale height of the neutral atmosphere. For the potential used here and for (0.2, 20 eV) particles, which is the range of energy of the coronal fast particles, σ_d is equal to $\sim 7 \times 10^{-16}$ cm^2 (Johnson et al., 2000). On the dayside, $H = 22$ km and the exobase altitude is $\sim$ 180 km (172 km according to Zhang et al., 1993a). Actually most of the fast recoil particles reaching 400 km in altitude have a radial speed around 2.0 km s^{-1} at 200 km in altitude which corresponds to an energy of 0.4 eV. Fig. 2 presents the average number of collisions that a fast recoil particle of radial speed 2.0 km s^{-1} at a given altitude makes in our model between this altitude and 400 km. The solid line without a symbol has been obtained by averaging over the half sphere, the circles correspond to the polar regions ($\phi = [0, 2\pi]$ and $\theta = \pi/2$), the cross line to the subsolar region ($\phi = 0$ and $\theta = \pi/2$) and the square line to the nightside region ($\phi = \pi$ and $\theta = 0$). From Fig. 2 an escaping particle of radial speed 2.0 km s^{-1} will make 0.3 energy transfer collisions before reaching 400 km losing, on the average, $\sim$ 20% of its energy, roughly consistent with the definition of an exobase. The estimate of the number of collisions above a given altitude varies across Mars being smaller in the polar and nightside regions which is due to the position and angle distribution of the primary impacting particles.

Fig. 3 presents the number of collisions of the fast recoils (> 0.07 eV) cm^{-3} s^{-1} (gray lines with opened symbols) and the density of recoils (dark lines with filled symbols) at three different positions in the atmosphere as a function of the altitude. The three positions are indicated using the same legend as in Fig. 2. It is seen that below 160 km the fast recoil population decreases due to rapid thermalization. A comparison between the three gray lines shows that most of the collisions happen in the subsolar regions below 200 km with a peak at 180 km for the polar and nightside regions. The dark solid lines indicate that the density of recoils in the polar regions is as high as in the subsolar regions for altitudes greater than 250 km. This illustrates the fact that the sputtered particles in the subsolar regions are redistributed in the direction of the nightside hemisphere. That is, the

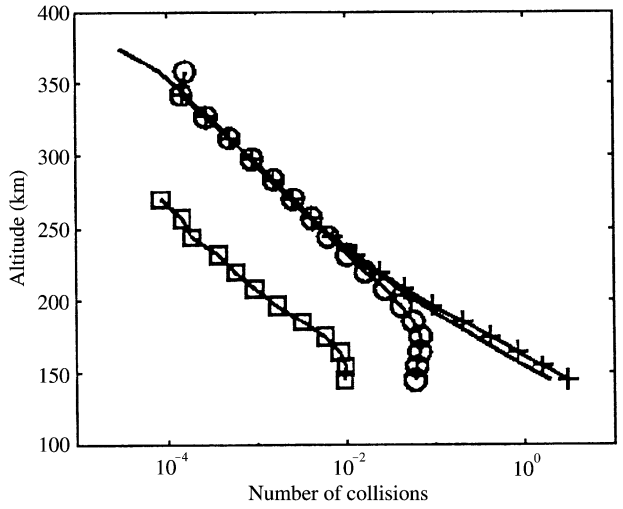

Fig. 2. Present epoch (solar minimum-3D MC simulation): Number of collisions made by a recoil particle of radial speed 2.0 km s^{-1} moving from the indicated altitude to 400 km. Solid line without symbol: average on the half-sphere of the domain of calculation. Line with crosses: subsolar regions. Line with circles: polar regions. Line with squares: midnight regions.

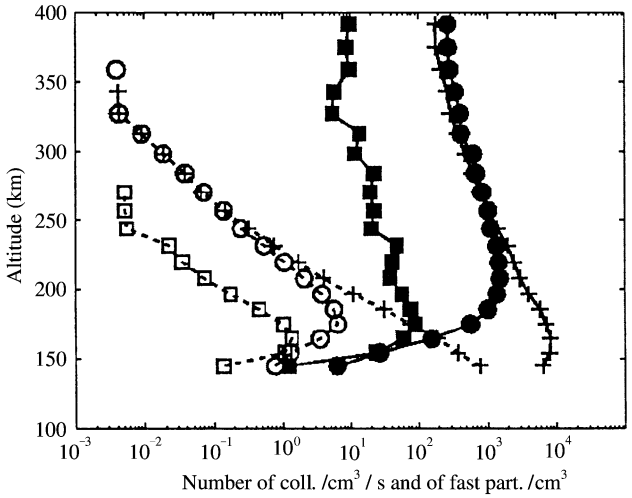

Fig. 3. Present epoch (solar minimum-3D MC simulation): Number of collisions per second and cm^3 (gray lines with opened symbols) and density of recoil particles per cm^3 (dark lines with filled symbols) as a function of the altitude. The different lines correspond to subsolar point (crosses), polar (circles) and nightside (squares) regions.

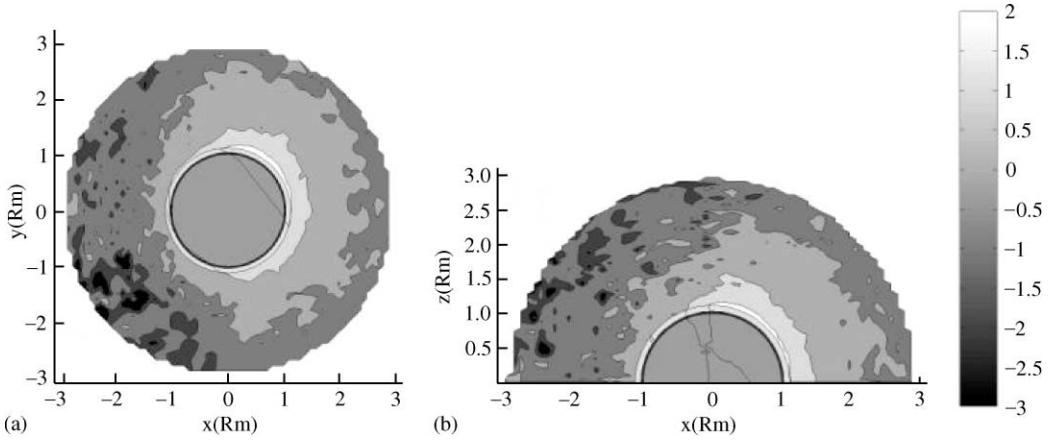

Fig. 4. Present epoch (solar minimum-3D MC simulation): Density of sputter produced coronal particles. The scale bar is in base 10 logarithm of the density in cm^{-3}. (a) In the equatorial plane. (b) In a plane perpendicular to the equatorial plane along the Mars/Sun axis. Mars is represented by the full and half circle in the center of each figure. Mars' rotation vector is directed towards the reader in Fig. 4a and towards the positive z axis in Fig. 4b.

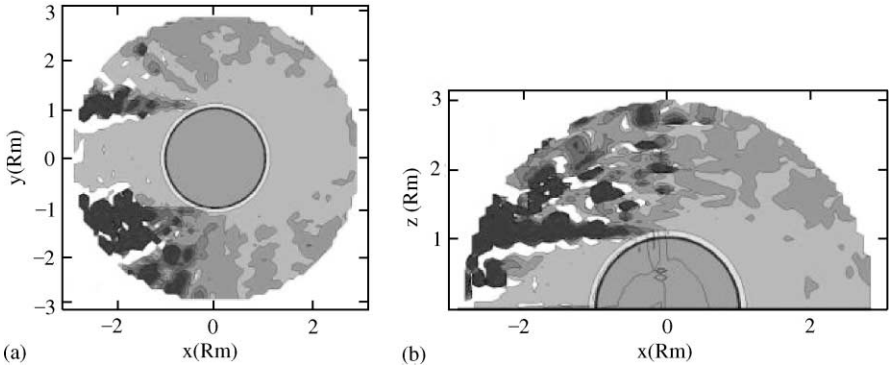

Fig. 5. Present epoch (solar minimum-3D MC simulation): Average energy of sputter produced coronal particles. (a) In the equatorial plane. (b) In a plane perpendicular to the equatorial plane along the Mars/Sun axis. The clearest regions correspond to energy lower than 2 eV (less than the escaped energy), the following darker one to energy larger than 2 eV and lower than 4 eV. The darkest regions corresponds to energy from 4 eV to more than 40 eV.

density in the nightside is due to ballistic particles which return to the atmosphere.

The simulation was also used to obtain the sputtering yield, which is the ratio of the total number of escaping particles to the total number of incident ones reaching the exobase. This was found to be equal to 2.9 (8387 simulated particles escaped due to 2898 incident particles). For comparison, Johnson et al. (2000) used a 1D model with the same scattering function, and obtained ~ 3.9 but added in ~ 1.3 due to the single collision ejection in the corona, directly treated here. In fact, we find that although a large proportion of the escaping particles come from atmospheric regions bombarded by particle with tangential incident angle (from regions around $\phi = \pm\pi/2$ and $\theta \in [\pi/5, \pi/2]$), the analytic correction made by Johnson et al. (2000) is too large.

The calculation also gives the enhancement in the corona density due to the sputtering of the neutral atmosphere by pick-up ions. Fig. 4 presents the density in the corona in two planes: the (xy) plane in Fig. 4a and the (xz) plane in Fig. 4b. The order of magnitude is in good agreement with the 1-D analytic results of Johnson and Luhmann (1998) for the subsolar regions and low altitudes. For present solar minimum conditions, the enhancement of the density due to the sputtering is negligible compared to dissociative-recombination of ionospheric O_2^+ (Zhang et al., 1993b; Kim et al., 1998). But Fig. 4a shows that due to the rotation of Mars the coronal density is not spherically symmetric and is somewhat larger in the dusk regions than in the dawn regions. The results also show that in the polar regions (Fig. 4b) and in the dusk regions (Fig. 4a) the enhancement in the density due to the sputtering has to be taken into account in order to accurately estimate the direct sputter loss from these regions.

Fig. 5 presents the average local kinetic energy of the sputtered particles inside the corona for the same two planes as in Fig. 4. The average energy in the corona (between the exobase and $2R_m$) is 15 eV per particle with the escaping particles having an average energy equal to 24 eV and the bound ballistic particles of average energy equal to 0.26 eV. Out of the equatorial regions, the high-energy

particles are in the "shadow" of the polar regions and the ballistic ones populate the subsolar regions and the tail. In the equatorial regions, the high-energy particles are mainly in the "shadow" of the dawn and dusk regions. The high-energy particles are more spread in the dawn regions than in the dusk regions because of Mars' rotation. This confirms the discussion above that sputtering efficiently produces energetic recoils and escaping particles when incident particles penetrate the atmosphere with angles close to tangential. It emphasizes, therefore, the importance of accurately describing these regions. The absence of a correlation between Figs. 4 and 5 indicates that the main component of the corona is the low energy particles. Compared to the results of Zhang et al. (1993a) and Kim et al. (1998), the population in the corona due to the sputtering might be distinguished by an in situ measurement from the population produced by the dissociative-recombination of O_2^+ ions, for which the energies are lower than 5 eV.

3.2. *3EUV*: ∼ 2.5 Gyr *ago*

3.2.1. *Description of the atmosphere heating due to the sputtering*

In order to first describe the heating of the neutral atmosphere due to the bombardment by pick-up O^+ ions we used a 2D DSMC model without any energy threshold below which particles are not followed. 6×10^6 simulated particles were followed each representing 10^{19} atmospheric atoms, considered all to be O atoms as discussed. Since a 2D model does not allow us to take into account Mars' rotation, we limit our simulation to 5.6 h (a 1/4 of one Mars' rotation) in order to use a realistic total incident flux. The 2D is convenient since heating due to the bombardment can be obtained with fewer incident particles than needed to estimate the loss of atmosphere or the enhancement of the coronal density. Indeed, the diffusion of the energy inside the atmosphere is determined by all the atmospheric particles whereas only few sputtered particles reach the exobase altitude for each incident particle. 100 incident particles are simulated which is enough to determine the difference between the polar and equatorial regions due to the geometry of the incident flux. The results are applicable above the exobase, but do not provide an accurate description of the full corona ($\sim 2R_m$). To obtain such results several days have to be simulated to take into account Mars' rotation.

The domain used in this simulation corresponds to the plane $\theta = \pi/2$ in Fig. 1 (plane xy). We limit the calculation to a region between $\phi = 0$ (subsolar regions) and $\phi = 4\pi/5$ (nightside regions) and between 150 and 600 km with ballistic particles tracked up to $2R_m$. Since the incident flux is symmetric around a Sun/Mars axis, we only describe half the atmosphere. The collisional domain between 150 and 600 km and $\phi = 0$ and $\phi = 4\pi/5$ is divided into 30×20 cells, respectively, in the radial and latitudinal directions. Mirror conditions are used at $\phi = 0$ and $\phi = 4\pi/5$. A mirror condition at $\phi = 4\pi/5$ has no influence on the result since no significant effect due to the sputtering are observed on the nightside of the atmosphere. Actually, the heat flux on the dayside is null largely before $\phi = 4\pi/5$. The particles which cross either 150 km or $2R_m$ from the surface are suppressed. The particles between 600 km and $2R_m$ from the surface are assumed to be ballistic and do not collide until they return to 600 km. Boundary conditions deduced from the solar maximum condition solution of Bougher et al. (1999) are imposed at 150 km. A temperature from 280 K on the dayside to 200 K on the nightside and a constant density of 10^{10} cm^{-3} of O atoms are used to define these boundary conditions. These bottom boundary conditions allow us to take into account the EUV and UV heatings which occur below 150 km. The initial atmosphere is deduced from the 3EUV solution of Zhang et al. (1993a). This choice does not significantly influence the results.

Figs. 6a and b present the profiles of temperature after 5.6 h of bombardment. Fig. 6a presents the profiles of the temperature with respect to the altitude r along the 5 lines plotted in Fig. 6b, which also gives the 2D distribution of the temperature. The large gray half-sphere in Fig. 6b is Mars' surface whereas, the half-dark ring is the Martian atmosphere below 150 km in altitude which is not influenced by the incident flux. Above this ring, the calculated profile of the temperature is plotted. On the left side of the Fig. 6b (dayside), temperatures higher than 300 K (up to ∼ 350 K) are obtained, whereas, on the right side around $\phi = 4\pi/5$ a nearly isothermic temperature profile of 200 K is found, confirming that this side of the atmosphere is not influenced for the bombardment geometry assumed here. On the dayside, there is a variation of ∼ 80 K going from 150 to 600 km. The heating produced by the incident flux is seen to be of the same order or higher than the one produced by the EUV and UV heating for the 3EUV epoch as predicted by Zhang et al. (1993a). Indeed, we obtained a dayside exospheric temperature of 350 K whereas these authors found a temperature of 330 K. The heating due to the bombardment extends below 220 km in the subsolar regions (in good agreement with Luhmann and Kozyra, 1991).

Fig. 7 provides the profiles of the density vs. the altitude for different regions of the atmosphere. The different lines correspond to the legend used in Fig. 6a. The squares (nightside) correspond to the isothermic profile shown in Fig. 6a. The density in the subsolar region, represented by the crosses, is more than an order of magnitude higher at 600 km than the one predicted profile (solid line without symbol, Zhang et al., 1993a). From Figs. 6a and 7, we can estimate the exobase altitude again using $n/(\sigma_d H) = 1$. For the sputtered particles (0.2, 20 eV) the corresponding momentum transfer cross section is equal to 7×10^{-16} cm^2. The scale height H deduced from the temperature profile is equal to 28 km on the dayside and to 47 km on the nightside and the theoretical exobase altitude from the previous definition is then equal to about 300 km on the dayside (216 km according to Zhang et al., 1993a) and around

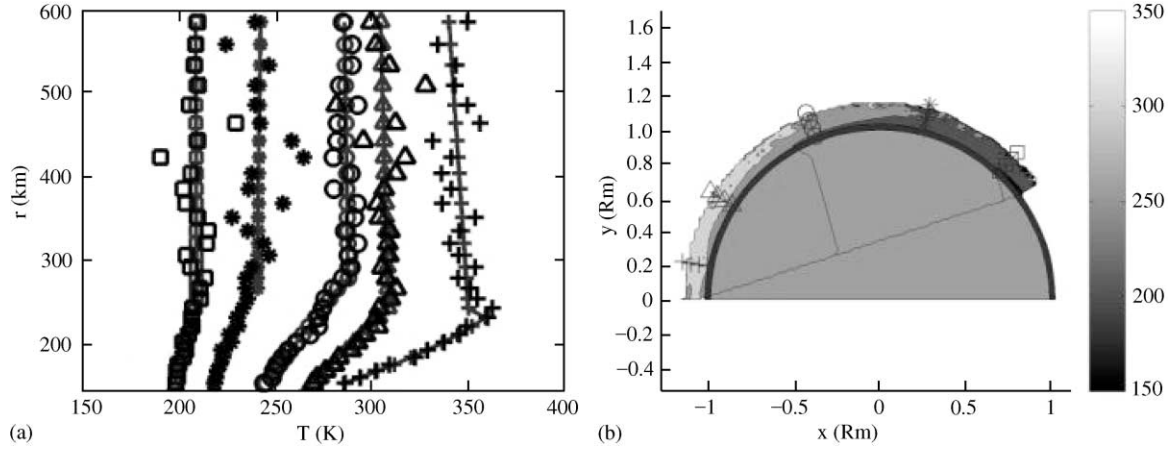

Fig. 6. Earlier epoch (2D DSMC simulation): (a) Temperature profiles of the neutral atmosphere with respect to the altitude. The different lines are profiles obtained at different latitudes of the Mars atmosphere as indicated in (b) (from left to right at $\phi = \pi/20$, $\pi/5$, $2\pi/5$, $3\pi/5$ and $3\pi/4$). (b) 2D temperature profiles of the neutral atmosphere (in K).

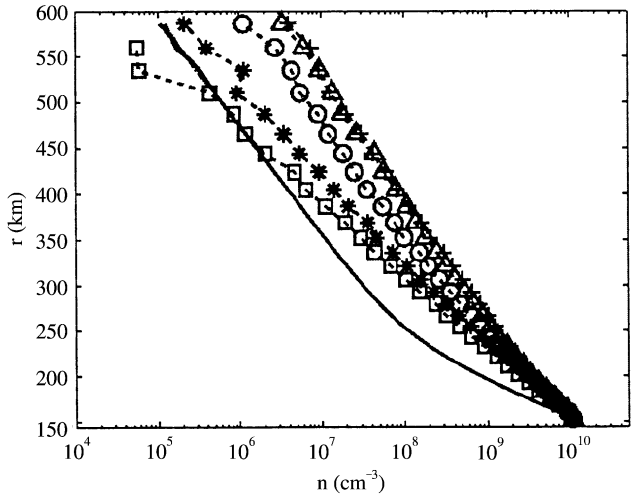

Fig. 7. Earlier epochs (2D DSMC simulation): Density profiles of the neutral atmosphere. Same legends as in Fig. 6. The solid line without symbol is the profile obtained by Zhang et al. (1993a) for the same epoch.

260 km on the nightside. Global high wind speeds are associated with the difference in density from day to night sides. The region of highest latitudinal speed is at 600 km just before the polar region and corresponds to winds of 156 m s^{-1}. For comparison, Bougher et al. (1999) have obtained for solar maximum wind speed of 260 m s^{-1} in the same region. The sputtering process at this epoch is, therefore, nearly as efficient as the EUV and UV flux in determining the properties of the exobase region and could be also important at solar maximum.

3.2.2. The sputtered population

A model of the Mars atmosphere heated by the incident flux in the 3EUV epoch was described in the previous subsection. In order to fully describe the corona up to $2R_m$ a 3D calculation is needed. For night to dayside, we used the profiles of the density and temperature which are interpolated from the solar maximum condition profiles of Bougher et al. (1999) for the nightside and the dashed lines with crosses in Figs. 6a and 7 for the dayside. On the nightside, the estimate made by Bougher et al. (1999) is more accurate than the results obtained above which ignore heat loss other than by atom transport and escape, whereas, on the dayside the heating due to the sputtering dominates. As for the 1EUV case, here 3.0 rotations of Mars have been simulated to reach a stationary state in terms of coronal density and yield. The background atmosphere consists of 2×10^{34} O particles and the weight factor used in this simulation is 3×10^{27}. 3112 incident particles were followed and the energy threshold used here is 0.11 eV (or $\sim$ 1100 K). For these tracked recoils the coronal density is accurately estimated in this simulation above 610 km. Below this altitude, the coronal density can be extrapolated from the results obtained in the previous subsection.

Fig. 8 gives the number of collision of an energetic recoil particle moving with a radial speed of 2.35 km s^{-1} from a given altitude to 600 km. The same legends defined in Fig. 2 are used. Based on the same maximum impact parameter as in the 1EUV simulation, Fig. 8 shows that a fast recoil particle of radial speed 2.35 km s^{-1} will make in an average 0.64 collisions between 300 and 600 km. The 2.35 km s^{-1} speed is the average speed of the ballistic particles reaching 600 km and corresponds to a kinetic energy of 0.46 eV. Around 0.2 eV is needed for a particle to go from 300 to 600 km and 0.26 eV is the average energy of the ballistic particles inside the corona. For the universal potential (Ziegler et al., 1985) and the cutoff chosen (2.5 Å), above 350 km 0.46 eV atoms will make 0.2 collisions with atmospheric atoms losing on the average 10% of its energy. From the exobase altitude

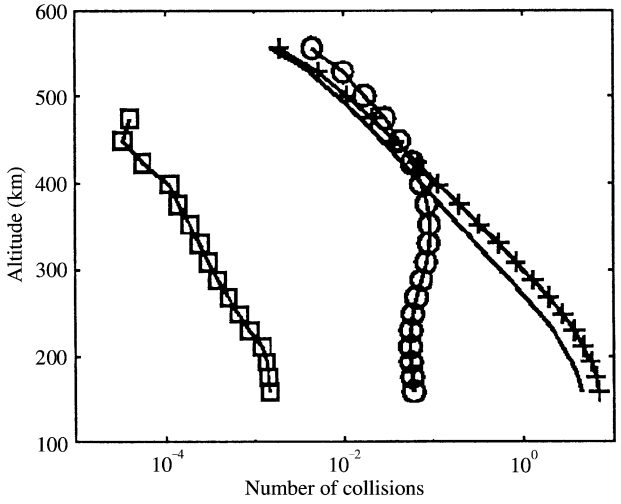

Fig. 8. Earlier epoch (3D MC simulation): Number of collision made by a recoil particle of radial speed 2.35 km s^{-1} in function of the altitude. Same format as in Fig. 2.

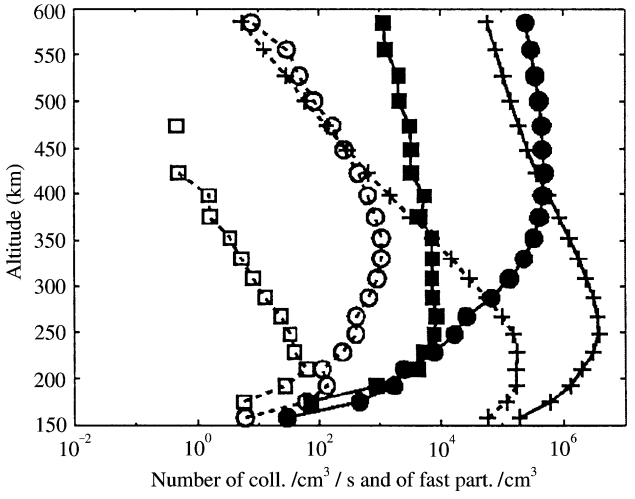

Fig. 9. Earlier epoch (3D MC simulation): Number of collision per second and cm^{-3} and density of recoil particles in cm^{-3} in function of the altitude. Same format as in Fig. 3.

(216 km) estimated by Zhang et al. (1993a), an atom of radial speed of 2.35 km s^{-1} will make on the average 3.0 collisions and lose all its energy before reaching 600 km.

In Fig. 9 the fast recoil densities are associated with the subsolar (crosses), polar (circles) and nightside (squares) regions. As in Section 3.1, the collisions between fast and atmospheric particles mainly occur in the subsolar regions. The remarks made for the density profiles in the subsolar and polar regions apply here also. The regions above the Martian poles are the most populated regions in the upper corona. The densities are not only higher than in the 1EUV but ballistic particles from the dayside contribute $\sim 10^3$ cm^{-3} at 610 km on the nightside. The density profile of fast particles thermalizes rapidly at low altitudes, so that the regions influenced by the pick-up ion bombardment are above 180 km.

The calculated yield is equal to 3.6 (corresponding to 11256 escaping for 3112 incident). The 1D model of Johnson et al. (2000) gave a yield of ~ 2.9 corrected to ~ 4.2 for coronal ejection. Again the correction to take into account the single collision sputtering was overestimated. As in the 1EUV case, the origin of the ejected atoms is in a large part from regions bombarded by grazing particles.

Figs. 10 and 11 present the density and energy of the coronal population issued from the bombardment of the atmosphere above 610 km in altitude. As for Figs. 4 and 5, cuts in the planes (xy) and (xz) are provided. The morphology of the coronal density is very similar to the 1EUV case (Fig. 5), but the density is from 2 to 3 order higher in the corona in this epoch. The maximal density of fast particles at 600 km is 10^5 cm^{-3} in the plane (xz) (Fig. 10b) and corresponds to polar regions as shown in Fig. 9. In the plane (xy) (Fig. 10a) the maximum is $10^{5.7}$ cm^{-3} and corresponds to dusk regions. This is much larger than the analytic 1D calculation made by Johnson and Luhmann (1998) who found $10^{4.5}$ cm^{-3} at 600 km in the subsolar region using the Zhang et al. (1993a) atmosphere. It is also consistent with the results obtained in previous subsection (Fig. 7) showing density of 10^6 cm^{-3} at 600 km on the dayside. The 3D picture of the corona density allows us to determine the density in the nightside and to obtain a more realist dependence of the density on altitude. For instance, Johnson and Luhmann (1998) overestimate the density by an order of magnitude at $2R_m$, whereas we find a higher density in the equatorial dusk regions at 600 km as shown in Fig. 10a. The density inside the corona due to the sputtered particles is shown here to be of the same order of magnitude as the density of oxygen due to the dissociative recombination of the O_2^+ (Zhang et al., 1993b), and is even higher than that estimate in the polar and dusk regions. Fig. 11 provides the local average energy of the coronal particles. As for Fig. 5, the asymmetry of the energy distribution is due to Mars' rotation. The average energy for the recoil particles inside the corona is equal to 9 eV, with an average energy for the escaping population equal to 13 eV in (xz) and to 9 eV in (xy) and for the ballistic population equal to 0.26 eV. As for the 1EUV case, the highest energy atoms are in the shadow of the dawn and polar regions and the lowest energetic particles populate the tail and the subsolar regions. The average energy at the 3EUV epoch is lower than at the 1EUV epoch because the energy of the incident particles is more easily spread in the denser atmosphere. The lack of a correlation between Figs. 10 and 11 indicates that the lowest energy particles are the main population in the corona. As for the 1EUV case, the average energy of the population sputtered in the corona is significantly higher than that from dissociative-recombination < 5 eV for present solar maximum conditions (Kim et al., 1998). It may be possible to distinguish the neutral coronal population produced by the sputtering from the dissociative-recombination corona during solar maximum, which is roughly an intermediate case between the 1EUV and the 3EUV epochs. The neutral

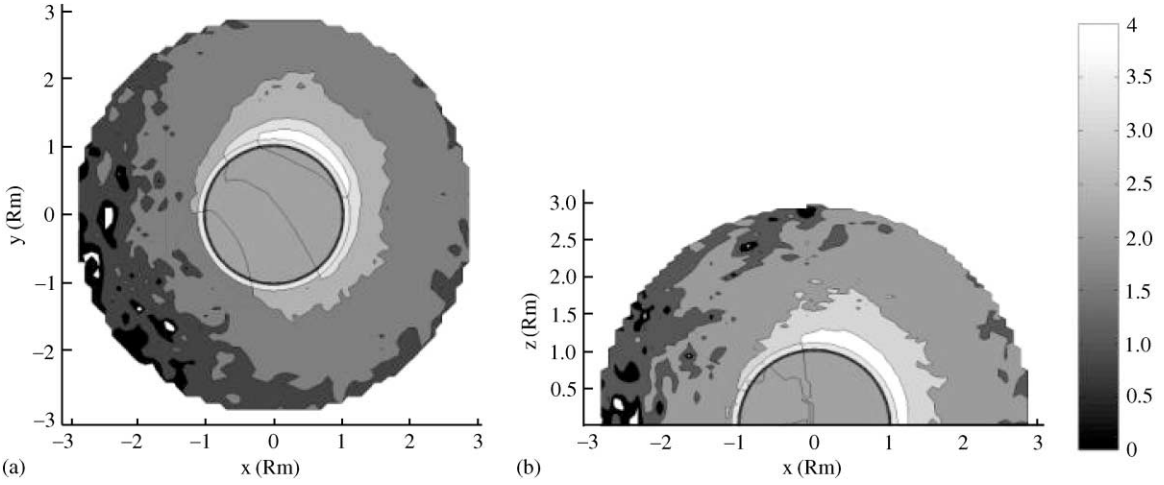

Fig. 10. Earlier epoch (3D MC simulation): Density of sputter produced coronal particles. The scale bar is in base 10 logarithm of the density in cm^{-3}. (a) In the equatorial plane. (b) In a plane perpendicular to the equatorial plane along the Mars/Sun axis.

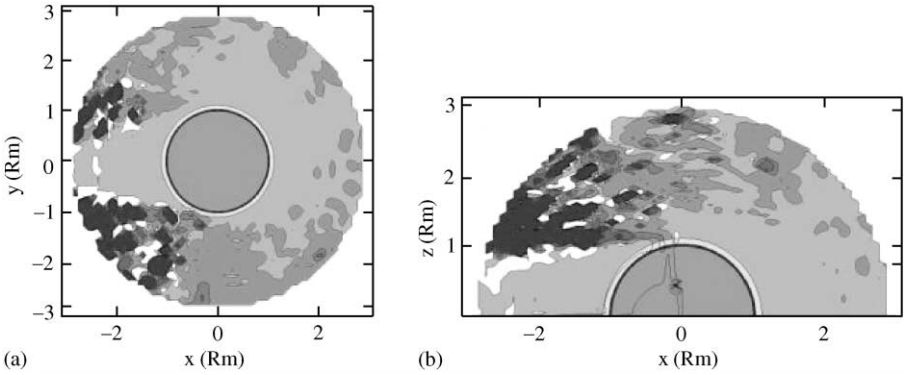

Fig. 11. Earlier epoch (3D MC simulation): Average energy of sputter produced coronal particles. (a) In the equatorial plane. (b) In a plane perpendicular to the equatorial plane along the Mars/Sun axis. Same format as in Fig. 5.

coronal density is roughly doubled by the sputter produced population compared to the estimations made by Zhang et al. (1993a). If we suppose that the density of ionized particles is roughly also doubled, the ionopause altitude is then roughly increased by $H \ln 2 \simeq 28$ km where H is the scale height (~ 47 km on the dayside). In the end, the density of ionized coronal particles above the ionopause will be roughly the same but the ionopause altitude higher, so that the total number of ionized particles will be larger. Moreover, since the sputter produced particles are on the average more energetic than those from dissociative-recombination, the sputtering becomes more important with increasing ionopause altitude.

4. Concluding remarks

We present in this paper the first 3D picture of the effect of the solar wind pick-up ions on the atmosphere of Mars. Two periods of Mars history are considered: one, present solar minimum and the other 3 times that EUV flux suggested to be ~ 2.5 Gyr ago. The process described in this paper is the sputtering of the atmosphere by ions picked up by the interplanetary magnetic field frozen inside the solar wind (Luhmann and Kozyra, 1991). It has been shown in previous studies (Jakosky et al., 1994; Kass and Yung, 1995; Johnson et al., 2000) that such process could significantly contribute to the Mars atmospheric loss. Johnson and Luhmann (1998) have shown that a potential feedback process associated with sputtering has also to be taken into account to accurately estimate the total loss of atmosphere. The sputtering requires development of a 3D simulation describing the trajectories of the incident ions around Mars (Brecht, 1997a, b) and the interaction of these particles penetrating the Martian atmosphere.

To compare with previous 1D studies, we used the model of incident flux of pick-up ions by Luhmann et al. (1992). For present solar minimum conditions, the heating due to the sputtering is small so we only consider the populations sputtered by the incident particles reaching altitudes higher

than the ionopause. Above this altitude these neutral particles can be ionized (Zhang et al., 1993b) and then can be accelerated by the solar wind fields and removed from Mars or they can be accelerated and reimpact the atmosphere. This bombardment can cause additional atoms to escape the gravity field of Mars. For the earlier epoch, the heating due to the incident particles is not negligible compared to the EUV and UV heating and is simulated with a full 2D Direct Simulation Monte Carlo model. For both epochs, the sputtered population reaching the corona above the ionopause is described by using a 3D Monte Carlo model.

We showed that in the 3EUV epoch the exobase altitude, here estimated as the altitude where the mean free path and the density scale height are equal, is around 300 km, significantly higher than the $\sim$ 216 km estimate of Zhang et al. (1993a) who only considered the UV and EUV heating. This increase is due to the heating by the incident pick-up ion flux and is a lower bound since the H^+ heating has been neglected. We also calculated the number of collisions per recoil particles in the corona showing that the collisions should not be ignored above the nominal exobase. As an example, above 180 km which is the exobase altitude calculated by Zhang et al. (1993a) for present solar minimum conditions, a sputtered particle loses by collisional energy transfer with the background around 20% of its energy before reaching the ionopause. For the earlier epoch, on the dayside, collisions can be neglected only above 350 km.

For both epochs we provide an estimate of the yield: the rate between the number of escaping neutral O particles to the number of incident ones. We found for present solar minimum a total yield of 2.9 which is less than the 3.9 estimate Johnson et al. (2000) and for the 3EUV epoch a total yield of 3.6, less than the 4.2 yield estimate of Johnson et al. (2000). This difference can be explained by our more complete description of the geometry of the corona. Indeed using the 3D model we are able to accurately calculate the effect of the grazing ions which are very efficient at producing escape. This contribution was overestimated by Johnson et al. (2000). The loss of particles s^{-1} during these two epochs are 6.5×10^{23} O atoms/s in the 1EUV and 1.3×10^{26} O atoms/s during the 3EUV epoch. These values are slightly larger than the estimate made by Jakosky et al. (1994) who found 3×10^{23} O atoms/s in the 1EUV and 10^{26} O atoms/s during the 3EUV epoch. To this loss should be added the much larger loss due to direct O^+ pick-up ion loss and to exospheric O atom loss (Luhmann et al., 1992).

The coronal density calculated in this work confirms the importance of sputtering (Johnson and Luhmann, 1998). At present solar minimum, the enhancement of the coronal density due to the sputtered population is negligible compared to dissociative-recombination of O_2^+ (Kim et al., 1998; Hodges, 2000) except in the polar and dusk equatorial regions. In the earlier epoch, this density is of the same order in the corona or greater in the polar and dusks equatorial regions than the density predicted by Zhang et al. (1993a). The number of lost O^+ pick-up ions should therefore be underestimated in Zhang et al. (1993a), Luhmann et al. (1992) and Luhmann (1997). Moreover, the energy range of the sputtered particles compared to the energy range of the O atoms produced by dissociative-recombination of O_2^+ (Kim et al., 1998; Hodges, 2000) is larger. Dissociative-recombination of the O_2^+ ions provides coronal O atoms of energy lower than 5 eV whereas the sputtering of the atmosphere generates coronal particles of average energy around 15 eV at present solar minimum and of 9 eV in the 3EUV epoch. This difference is also important for the feedback process (Johnson and Luhmann, 1998) since it implies that these sputter produced particles populate larger distance from Mars than the dissociative–recombination process where they are more readily ionized.

Acknowledgements

This work was supported by the NASA's Planetary Atmosphere Program.

References

Acuña, M.H., et al., 1998. Magnetic field and plasma observations at Mars: initial results of the Mars Global Surveyor mission. Science 279, 1676–1680.

Acuña, M.H., et al., 1999. Global distribution of crustal magnetization discovered by the Mars Global Surveyor MAG/ER experiment. Science 284, 790–793.

Bird, G.A., 1994. Molecular Gas Dynamics and the Direct Simulation of Gas Flows. Clarendon Press, Oxford, England.

Bougher, S.W., Engel, S., Roble, R.G., Foster, B., 1999. Comparative terrestrial planet thermosphere 2. Solar cycle variation of global structure and winds at equinox. J. Geophys. Res. 104, 16,591–16,611.

Bougher, S.W., Roble, R.G., 1991. Comparative terrestrial planet thermosphere 1. Solar cycle variation of global mean temperature. J. Geophys. Res. 96, 11,045–11,055.

Brain, D.A., Jakosky, B.M., 1994. Atmospheric loss since the onset of the Martian geologic record: combined role of impact erosion and sputtering. J. Geophys. Res. 103, 22,689–22,694.

Brecht, S.H., 1997a. Hybrid simulations of the magnetic topology of Mars. J. Geophys. Res. 102, 4743–4750.

Brecht, S.H., 1997b. Solar wind proton deposition into the Martian atmosphere. J. Geophys. Res. 102, 11,287–11,294.

Carr, M.H., 1999. Retention of an atmosphere on early Mars. J. Geophys. Res. 104, 21,897–21,909.

Firsov, O.B., 1959. A qualitative interpretation of the mean electron excitation energy in atomic collisions. Zh. Eksp. Teor. Fiz. 36, 1517–1523 (Sov. Phys. JETP (Engl. Transl.) 36, 1076–1086, 1959) (in Russian).

Hodges, R.R., 2000. Distributions of hot oxygen for Venus and Mars. J. Geophys. Res. 105, 6971–6981.

Jakosky, B.M., Jones, J.H., 1997. The history of the Martian volatiles. Rev. Geophys. 35, 1–16.

Jakosky, B.M., Pepin, R.O., Johnson, R.E., Fox, J.L., 1994. Mars atmospheric loss and isotopic fractionation by solar-wind induced sputtering and photochemical escape. Icarus 111, 271–288.

Johnson, R.E., 1994. Plasma-ion sputtering of an atmosphere. Space Sci. Rev. 69, 215–253.

Johnson, R.E., Liu, M., 1996. The loss of atmosphere from Mars. Science 274, 1932.

Johnson, R.E., Luhmann, J.G., 1998. Sputter contribution to the atmospheric corona on Mars. J. Geophys. Res. 103, 3649–3653.

Johnson, R.E., Schnellenberger, D., Wong, M.C., 2000. The sputtering of an oxygen thermosphere by energetic O^+. J. Geophys. Res. 105, 1659–1670.

Kallio, E., Luhmann, J.G., 1997. Charge exchange near Mars: the solar wind absorption and energetic neutral atom production. J. Geophys. Res. 102, 22,183–22,197.

Kass, D.M., Yung, Y.L., 1995. Loss of atmosphere from Mars due to solar-wind induced sputtering. Science 268, 697–699.

Kass, D.M., Yung, Y.L., 1996. The loss of atmosphere from Mars: response. Science 274, 1932–1933.

Kim, J., Nagy, A.F., Fox, J.L., Cravens, T.E., 1998. Solar cycle variability of hot oxygen atoms at Mars. J. Geophys. Res. 103, 29,339–29,342.

Luhmann, J.G., 1997. Correction to "The ancient oxygen exosphere of Mars: implications for atmosphere evolution" by Zhang et al. J. Geophys. Res. 102, 1637.

Luhmann, J.G., Johnson, R.E., Zhang, M.H.G., 1992. Evolutionary impact of sputtering of the Martian atmosphere by O^+ pick-up ions. Geophys. Res. Lett. 19, 2151–2154.

Luhmann, J.G., Kozyra, J.U., 1991. Dayside pick-up oxygen in precipitation at Venus and Mars: spatial distribution, energy deposition and consequences. J. Geophys. Res. 96, 5457–5467.

McElroy, M.B., 1972. Mars: an evolving atmosphere. Science 175, 443.

Nagy, A.F., Cravens, T.E., 1988. Hot oxygen atoms in the upper atmospheres of Venus and Mars. Geophys. Res. Lett. 15, 433.

Pospiezalska, M.K., Johnson, R.E., 1992. Plasma heating of Io's atmosphere. Geophys. Res. Lett. 19, 949–952.

Pospiezalska, M.K., Johnson, R.E., 1996. Monte Carlo calculations of plasma ion-induced sputtering of an atmosphere: SO_2 ejected from Io. J. Geophys. Res. 101, 7565–7573.

Pepin, R., 1994. Evolution of the Martian atmosphere. Icarus 111, 289–304.

Smyth, W.H., Combi, M.R., 1988. A general model for Io's neutral gas clouds. II Application to the sodium cloud. Astrophys. J. 328, 888–918.

Wong, M.C., Johnson, R.E., 1995. A three-dimensional azimuthally symmetric model of the atmosphere of Io, 1., Photochemistry and the accumulation of a nightside atmosphere. J. Geophys. Res. 101, 23,243–23,254.

Zhang, M.H.G., Luhmann, J.G., Bougher, S.W., Nagy, A.F., 1993a. The ancient oxygen exosphere of Mars: implication for atmosphere evolution. J. Geophys. Res. 98, 10,915–10,923.

Zhang, M.H.G., Luhmann, J.G., Nagy, A.F., Spreiter, J.R., Stahara, S., 1993b. Oxygen ionization rates at Mars and Venus: relative contributions of impact ionization and charge exchange. J. Geophys. Res. 98, 3311–3318.

Ziegler, J.F., Biersack, J.P., Littmark, V., 1985. The Stopping and Ranges of Ions in Solids. Pergamon Press, New York.

Zuber, M.T., et al., 2000. Internal structure and early thermal evolution of Mars from Mars Global Surveyor, Topography and Gravity. Science 287, 1788.